Four-in-one interferometer for coherent and self-coherent detection

Jingshi Li,[1,*] Muhammad Rodlin Billah,[1] Philipp C. Schindler,[1] Matthias Lauermann,[1] Sven Schuele,[1] Stefan Hengsbach,[1] Uwe Hollenbach,[1] Juergen Mohr, [1] Christian Koos,[1] Wolfgang Freude,[1] and Juerg Leuthold[1,2]

[1] *Institutes IPQ and IMT, Karlsruhe Institute of Technology (KIT), 76131 Karlsruhe, Germany*
[2] *Institute of Electromagnetic Fields (IFH), ETH Zurich, CH-8092 Zurich, Switzerland*
[*] *jingshi.li@kit.edu*

Abstract: A compact micro-optical interferometer is presented that combines two optical 90° hybrids or, alternatively, four delay interferometers into one interferometer structure sharing one tunable delay line. The interferometer can function as a frontend of either a coherent receiver or of a self-coherent receiver by adjusting the waveplates and the delay line. We built a prototype on a LIGA bench. We characterized the device and demonstrated its functionality by successful reception of a 112 Gbit/s signal.

OCIS codes: (060.1660) Coherent communications; (060.5060) Phase modulation; (060.2330) Fiber optics communication.

References and links

1. C. R. Doerr, P. J. Winzer, Y.-K. Chen, S. Chandrasekhar, M. S. Rasras, L. Chen, T.-Y. Liow, K.-W. Ang, and G.-Q. Lo, "Monolithic polarization and phase diversity coherent receiver in silicon," J. Lightwave Technol. **28**(4), 520–525 (2010).
2. J. Rahn, G. Goldfarb, H.-S. Tsai, W. Chen, S. Chu, B. Little, J. Hryniewicz, F. Johnson, W. Chen, T. Butrie, J. Zhang, M. Ziari, J. Tang, A. Nilsson, S. Grubb, I. Lyubomirsky, J. Stewart, R. Nagarajan, F. Kish, and D. F. Welch, "Low-power, polarization tracked 45.6 GB/s per wavelength PM-DQPSK receiver in a 10-channel integrated module," in Proc. Optical Fiber Communication Conference (OFC'10), paper OThE2 (2010).
3. C. R. Doerr and L. Chen, "Monolithic PDM-DQPSK receiver in silicon," in Proc. European Conference on Optical Communication (ECOC'10), post-deadline paper PD3.6 (2010).
4. Y. C. Hsieh, "Free-space optical hybrid," US Patent Application 02223932 A1 (2007).
5. C. Meuer, C. Schmidt-Langhorst, R. Bonk, H. Schmeckebier, D. Arsenijević, G. Fiol, A. Galperin, J. Leuthold, C. Schubert, and D. Bimberg, "80 Gb/s wavelength conversion using a quantum-dot semiconductor optical amplifier and optical filtering," Opt. Express **19**(6), 5134–5142 (2011).
6. J. Li, K. Worms, R. Maestle, D. Hillerkuss, W. Freude, and J. Leuthold, "Free-space optical delay interferometer with tunable delay and phase," Opt. Express **19**(12), 11654–11666 (2011).
7. X. Liu, S. Chandrasekhar, and A. Leven, "Digital self-coherent detection," Opt. Express **16**(2), 792–803 (2008).
8. W. Menz and J. Mohr, "Mikrosystemtechnik für Ingenieure," Zweite erweitert Auflage, VCH Verlag (1997).
9. S. Schuele, S. Hengsbach, U. Hollenbach, J. Li, J. Leuthold, and J. Mohr, "Active modular microsystems based on Mach-Zehnder interferometers," in Proc. SPIE Photonics Europe, Nonlinear Optics and its Applications **7716**, paper 7716–36 (2010).
10. G. Bosco and P. Poggiolini, "On the joint effect of receiver impairments on direct-detection DQPSK systems," J. Lightwave Technol. **24**(3), 1323–1333 (2006).

1. Introduction

For coherent communication to become practical, cheap coherent and self-coherent receivers that require as few elements as possible are needed. Many research groups have been investigating solutions based on integrated optics [1–3]. Integrated optics solutions offer small dimensions and possible co-integration with photo-diodes and electronic circuits. Yet, the most common technique for commercial devices [4] is still based on free-space optics because of the stability and high quality of the optical characteristics. Another advantage of free space solutions is the large operation wavelength range (several 100 nm, e.g., from 1300 nm [5] to

#185858 - $15.00 USD Received 22 Feb 2013; revised 17 May 2013; accepted 17 May 2013; published 24 May 2013

1550 nm [6]), and the option to continuously tune the time delay which is useful for self-coherent reception [6].

In contrast to integrated optics where many elements can be co-integrated, free-space optics is limited in the number of physical components due to space and cost restrictions. A polarization and phase diverse coherent receiver requires 2 optical 90° hybrids. Each optical 90° hybrid comprises several beam splitters, phase shifters and reflectors for beam alignment, see Fig. 1(a). A self-coherent receiver consists of either a delay line plus 2 optical 90° hybrids or 4 delay interferometers (DI), see Fig. 1(f) and 1(g). The latter requires 3 additional time delay arms in comparison to the former. Each DI needs to be controlled individually in order to match the signal's symbol rate (1 / Ts), and the phase of each DI needs to be adjusted to guarantee orthogonality between the in-phase (I) and quadrature (Q) DIs. Therefore, efforts to reduce the number of hybrids / DIs are necessary. One method is to use polarization insensitive hybrids / DIs and separate the polarizations at the outputs [7]. However, polarization-insensitive hybrids / DIs are intricate to fabricate. Additionally, because the polarizations are separated at the outputs, the scheme is very sensitive to unwanted polarization rotation or birefringence before the polarizations are separated. Any spurious polarization rotation or birefringence would directly translate into coherent polarization crosstalk. The second method is to spatially separate the two polarizations at the input and lead them in parallel into the same optical components, which can be easily assembled with free-space optics. However, this method requires highly accurate optical alignment.

Being a high precision X-ray lithography technology, LIGA technology (*li*thography, *ga*lvanic electroplating, molding) [8] can be used for fabricating passive alignment structures for optical elements with tolerances down to 200 nm and maximum heights up to 1 mm. By snapping micro-optical elements into the LIGA alignment structure, one can reduce the dimensions of the setup [9]. In addition, good optical performance is guaranteed by the mature coating technology of free-space optical elements.

In this paper we introduce a compact micro-optical interferometer in LIGA technology. The number of optical components used in the interferometer is minimized by reusing the optical interfaces up to four times. Our scheme folds two optical 90° hybrids for a coherent receiver and four delay interferometers for a self-coherent receiver into a single interferometer structure with one single time delay adjustment. It can be switched from a polarization diverse coherent receiver to a polarization diverse self-coherent receiver by simply adjusting the birefringent waveplates.

2. Interferometer principle and structure

To better explain the path towards a component reduction for coherent and self-coherent receivers we begin with a description of the basic structures.

In a conventional optical polarization and phase diverse coherent receiver as shown in Fig. 1(a), the incoming signal (blue line) is split by a polarization beam splitter (PBS) in two orthogonal polarizations, namely *s* (perpendicular to the incident plane, solid) and *p* (parallel with the incident plane, dashed) polarization, each of which is then superimposed to a local oscillator (LO, red line) at the same polarization in an optical 90° hybrid. At the outputs, the in-phase (I) and quadrature phase (Q) components of the sum and difference of two beams are received by pairs of balanced detectors.

In a self-coherent receiver, instead of the local oscillator, a delayed copy of the signal is combined with itself in an optical 90° hybrid as shown in Fig. 1(f), or in two delay interferometers with orthogonal phase offset as in Fig. 1(g).

#185858 - $15.00 USD Received 22 Feb 2013; revised 17 May 2013; accepted 17 May 2013; published 24 May 2013

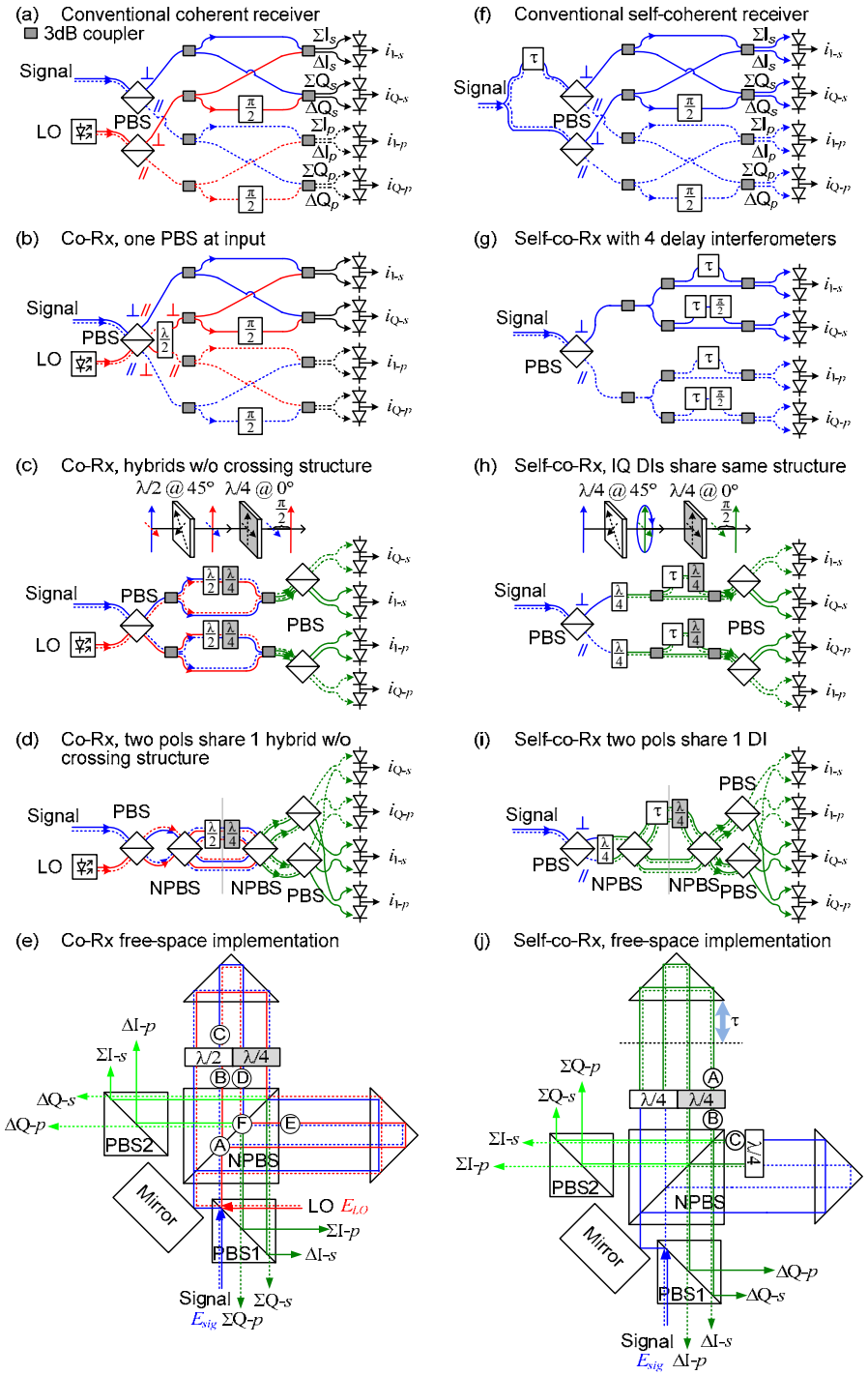

Fig. 1. Schematic illustration of a polarization and phase diverse coherent receiver and self-coherent receiver frontend. The left column presents from top to bottom the transformation from a conventional coherent receiver (a) to a free-space optics interferometer configuration (e). The right column (f) to (j) presents a similar transformation for the self-coherent receiver. Both receiver types can be realized with the same device. ⊥: *s*-polarized light; //: *p*-polarized light.

#185858 - $15.00 USD Received 22 Feb 2013; revised 17 May 2013; accepted 17 May 2013; published 24 May 2013

Therefore a polarization and phase diverse coherent receiver requires 2 PBS, 8 couplers, and 2 phase shifters. A polarization and phase diverse self-coherent receiver requires 2 or 1 PBS, 8 or 10 couplers, 1 or 4 tunable delay lines and 2 phase shifters.

Here, we will show how to build a receiver frontend that only requires 2 PBS, 1 non-polarizing beam splitter (NPBS), 3 reflectors for folding beams to reuse optical surfaces, 3 waveplates, and 1 tunable delay line. Thus, we can reduce the total number of optical components from 12…17 (not taking into account the reflectors that typically are needed to align the beams with the components) to a number of only 7 optical components plus 3 reflectors. At the same time, this device can be switched between a coherent receiver and a self-coherent receiver frontend.

Coherent receiver. We first reduce the number of PBSs at the input from 2 to 1. In Fig. 1(b), the signal and the LO are led into the PBS from different sides. After the PBS, a half waveplate (HWP) at 45° rotation with respect to the PBS is used to flip the split polarization states of the LO to their orthogonal states. Then the signal and LO at the same polarizations are mixed in the optical 90° hybrids.

In free-space optics, the crossing structure in the middle of the optical 90° hybrid of Fig. 1(b) requires several reflectors. To further reduce the number of optical elements, the optical 90° hybrid can be built in a different way, Fig. 1(c). After the PBS, the signals are split in two couplers. At one arm of each coupler, a HWP at 45° rotation with respect to the PBSs is introduced to convert the signal and LO onto their orthogonal polarizations. Thus the signal can be superimposed with the LO at the same polarizations at the second coupler. A quarter-waveplate (QWP) at 0° is positioned before the second coupler to provide the necessary 90° phase shift for creating the quadrature signal. Now we have again two optical hybrids after the input PBS. Compared to Fig. 1(b), three more waveplates and two more PBSs are required while saving four couplers, 2 phase shifters, and avoiding crossings.

The two optical hybrids can then be built into one optical hybrid configuration by spatially overlapping them as in Fig. 1(d). Here the couplers are realized by non-polarizing beam splitters (NPBS). By folding the configuration along the gray line in the figure, we finally get the interferometer in Fig. 1(e), where only 1 NPBS and 2 PBSs are needed instead of 2 NPBS and 3 PBS in Fig. 1(d).

Self-coherent receiver. Starting from Fig. 1(g), we first reduce the number of DIs from 4 to 2 as in Fig. 1(h). After the PBS, a QWP at 45° rotation with respect to the PBSs is introduced at each polarization to convert the linearly polarized light into circularly polarized light. The circularly polarized light has new *s* (green solid) and *p* (green dashed) components with equal power. They share the same DI and are separated at the outputs by PBSs. By using a QWP at 0°, 90° phase shift is introduced between the new *s* and *p* components, thus that one polarization forms an in-phase component (e.g., the dashed line) while the other forms a quadrature phase component (e.g., the solid line).

The two DIs can be combined within the same DI structure as in Fig. 1(i). Finally, the configuration can be re-arranged as a free-space optical interferometer with only one NPBS and two PBS as shown in Fig. 1(j). One may now compare the coherent receiver, Fig. 1(e) with the self-coherent receiver of Fig. 1(j). The only differences are in an exchange of waveplates and an additional waveplate, in a non-zero delay for the self-coherent receiver, and in a LO input for the coherent receiver. Thus both the configurations can be easily converted back and forth by using adjustable waveplates and a tunable delay. Tunable waveplates can be realized with liquid crystal cells, and the tunable time delay can be obtained by mounting the reflector onto a motor. A mathematic expression of the concept can be found in the appendix.

3. Free-space coherent and self-coherent receiver design and implementation

The free-space scheme comprises a micro-optical bench that serves as a guiding structure for high-precision alignment of the optical elements. The fabrication steps are as follows:

#185858 - $15.00 USD Received 22 Feb 2013; revised 17 May 2013; accepted 17 May 2013; published 24 May 2013

The micro-optical bench is designed and modeled with a ray-tracing tool, and the resulting structure exported as a CAD layout. Then alignment constructs are added around the optical micro-elements. The complete 3D volume assembly is then reduced to a 2D outline, which serves as input data for the X-ray mask.

First, a premask is manufactured using e-beam lithography. A gold layer with a height of about 2 µm is structured on a 4 µm thick titanium foil, see Fig. 2(a). In the next step, the premask is used for the production of a master mask. The master mask is an invar (nickel iron alloy with low thermal expansion) foil carrying the structured gold absorber layer with a height of about 25 µm, which is fabricated with gold electroplating, Fig. 2(b). Both gold layers absorb X-rays, while the titanium foil or the invar foil is essentially transparent. A foil with PMMA resist having a thickness of 610 µm is glued to the silicon wafer. After deep X-ray lithography, a developing process leads to high aspect ratio PMMA alignment structures in the micro-optical bench, Fig. 2(c). For mass production, such structures are strengthened with a nickel electroplating process, and the resulting nickel molding tool can be used for hot embossing. The complete process is often described as LIGA technology [8] (*li*thography, *ga*lvanic electroplating, molding).

Single benches with dimensions of 21 × 22 mm^2 are diced from the wafer by laser cutting using a pulsed NdYag laser. The dimension of the single bench may be further reduced if smaller optical elements were chosen instead of commercially available elements.

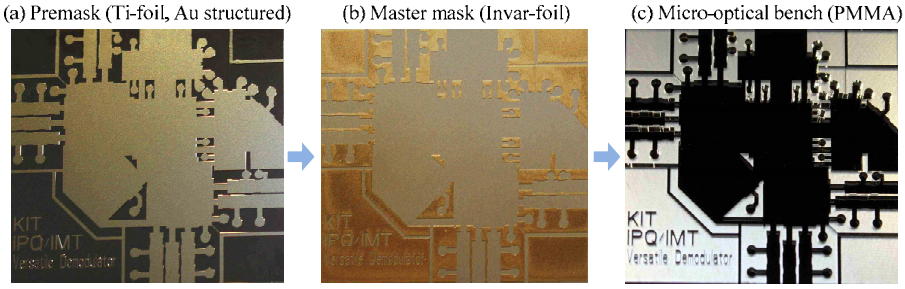

Fig. 2. Fabrication steps for the LIGA process. Pictures of the (a) premask (Ti-foil with Au structures), of the (b) master mask (invar-foil), and of the final (c) micro-optical bench (PMMA).

A prototype of micro-optical interferometer has been fabricated by positioning the optical elements using the alignment and guiding features of the micro-optical bench, see Fig. 3. Grin lenses with a diameter of 1 mm are used to couple the optical beams from and to the fiber. PBS and NPBS are chosen to be 5 × 5 × 5 mm^3 which is commonly available on the market. Porro prisms are coated with metallic coating on their orthogonal sides. One Porro prism is attached to a piezo-motor which acts as a tunable time delay and an adjustable phase shifter. A mirror cube is used to deflect the second polarization (*s* light) to the NPBS. Liquid crystal (LC) cells serve as waveplates whose birefringence can be changed by adjusting the applied voltage. Two LC cells have axes rotated with respect to the PBS eigenstates by −45°, and one has axes aligned with the PBS. The LC cells are positioned such that the beams reflected by the Porro prisms would only pass the waveplates once, as indicted in Fig. 1(e), 1(j) and Fig. 3(b). Finally, the optical elements are glued to the bench. The 8 outputs for the in-phase and quadrature components and the two polarizations are named ‘Out1’ to ‘Out8’. They correspond to different ports of the coherent and self-coherent receiver as listed in Table 1.

Table 1. Output numbering in coherent and in self-coherent receiver

Output number	Out1	Out2	Out3	Out4	Out5	Out6	Out7	Out8
Coherent	Σ*Q*-*p*	Δ*Q*-*p*	Σ*I*-*p*	Δ*I*-*p*	Σ*Q*-*s*	Δ*Q*-*s*	Δ*I*-*s*	Σ*I*-*s*
Self-coherent	Δ*I*-*p*	Σ*I*-*p*	Δ*Q*-*p*	Σ*Q*-*p*	Δ*I*-*s*	Σ*I*-*s*	Δ*Q*-*s*	Σ*Q*-*s*

#185858 - $15.00 USD Received 22 Feb 2013; revised 17 May 2013; accepted 17 May 2013; published 24 May 2013

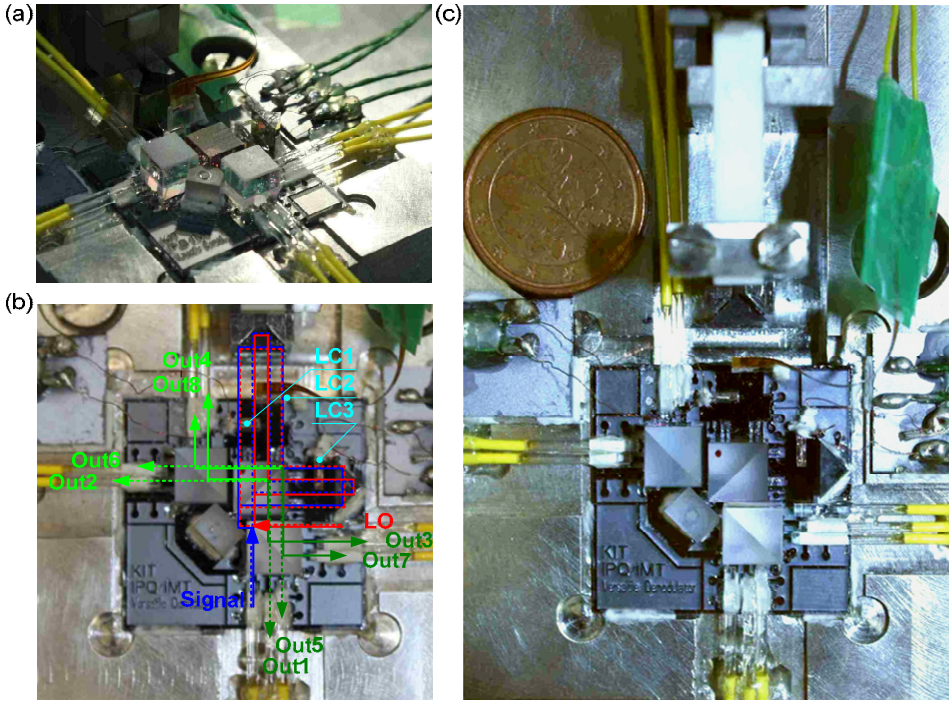

Fig. 3. Photograph of a complete micro-optical interferometer. (a) Side view; (b) Top view with beam paths; (c) Top view of a Euro cent and the complete micro-optical interferometer including the motor.

4. Characterization and testing

The free space receiver frontend was tested for its performance in a self-coherent and in a coherent receiver.

We first tested the device as a self-coherent receiver. For this purpose, the LC cells were adjusted to act as QWPs at –45° (LC1 and LC3), and as a QWP at 0° (LC2) as in our schematic of Fig. 1(j). The LC2 cell at 0° may also be used to compensate polarization dependent frequency shift (PDFS) within the setup [6]. The static performance of the micro-optical interferometer is characterized by wavelength-sweeping a C-band tunable laser with a wavelength resolution of 1.44 pm. The micro-optical interferometer is measured with the minimal and maximal free spectral range (FSR) by adjusting the piezo-motor to its farthest and closest position with respect to the Porro prism. In Fig. 4 we plot the spectral response of outputs Out1…Out8 at *p* and *s* polarization adjusted to a FSR of 17.5 GHz and 50 GHz. The outputs are named as in Table 1. We see that the outputs represent constructive and destructive ports of the I and Q components. The extinction ratios for all the outputs are larger than 18 dB, which is sufficient for signal reception [10]. The excess insertion losses for all the outputs are below 4 dB. The insertion losses for output 5, 6, 7 and 8 are slightly higher than for output 1, 2, 3, and 4. This is because the *s* polarization is deflected by the mirror cube which introduces extra absorption and misalignments. We conclude that the device keeps good extinction ratio and insertion loss over a tuning range of 17.5…50 GHz, corresponding to a delay tuning range of 20…57 ps. The device has potential to cover a larger time delay range, e. g., down to zero delay, by reducing the tunable path when dicing the chip.

#185858 - $15.00 USD Received 22 Feb 2013; revised 17 May 2013; accepted 17 May 2013; published 24 May 2013

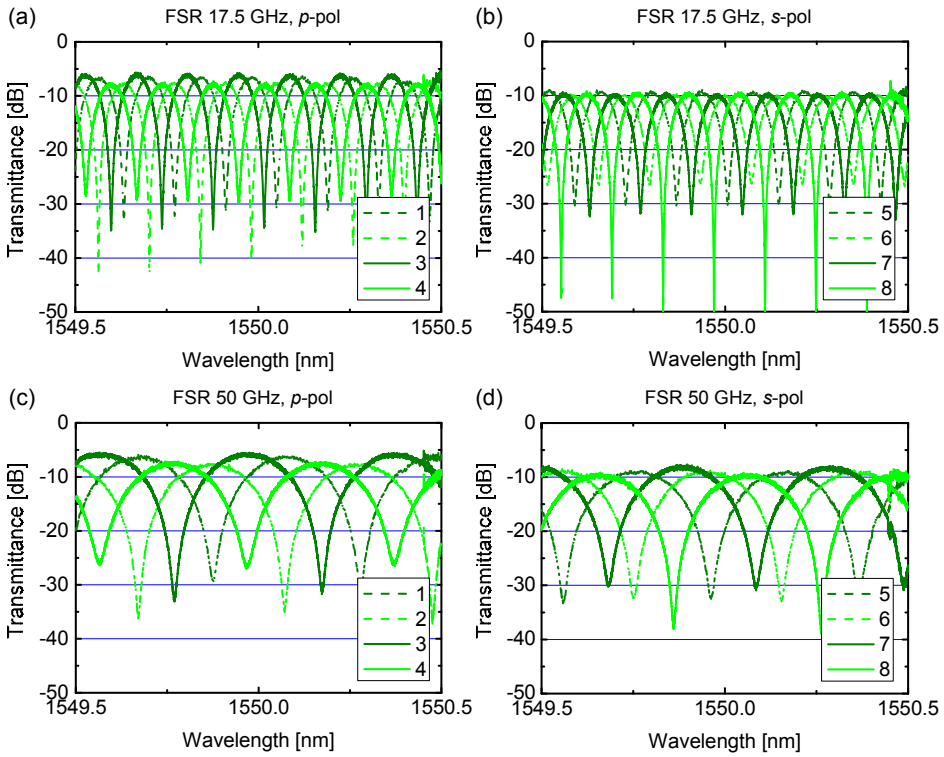

Fig. 4. Micro-optical interferometer as self-coherent receiver. Spectral responses of outputs 1 (dark green dashed line), 2 (light green dashed line), 3 (dark green solid line) and 4 (light green solid line) at *p*-polarization in a wavelength range 1549.5 nm … 1550.5 nm. Free spectral range (a) 17.5 GHz, and (b) 50 GHz. Spectral responses of outputs 5 (dark green dashed line), 6 (light green dashed line), 7 (dark green solid line) and 8 (light green solid line) at *s*-polarization for 1549.5 nm … 1550.5 nm. Free spectral ranges (c) 17.5 GHz and (d) 50 GHz.

The spectral response for various free spectral ranges (FSR) is measured in the C band. In Fig. 5, we present the spectral response for FSR = 25 GHz near 1527 nm, 1550 nm and 1565 nm at *p* and *s*-polarization. The device has similar performance over the full C band.

Table 2. Polarization extinction ratios for the outputs of micro-optical interferometer as coherent detection scheme.

Output number	Out1	Out2	Out3	Out4	Out5	Out6	Out7	Out8
Sig. Pol. ER [dB]	19.4	19.2	22	20.7	18.4	17.9	20	19.6
LO Pol. ER [dB]	19.5	18	25.3	23	22.2	19.6	20.9	18.2
Insertion loss difference [dB]	0.03	1.29	1.97	2.95	0.83	0.88	0.26	1.07

We then tested the micro-optical interferometer as a coherent receiver. One LC cell which was positioned previously at –45° (LC3) is now set to "neutral" so that it does not change the polarization states of the beams. The other LC cell at –45° (LC1) is set as a HWP so that it flips the linear polarization states of signal and LO to their orthogonal states. Polarization extinction ratios are measured by comparing the power of *p* and *s*-light at the outputs with either the signal input only, or with the LO input only. The polarization extinction ratios for all outputs are listed in Table 2. The minimal polarization ER is 17.9 dB. The insertion losses for signal and LO at each output are also compared. The maximal difference is to be seen at Out4, where a 2.95 dB power difference is measured. There is non-zero path difference between the upper and the right paths in Fig. 3(b) due to technological constrains of our present

#185858 - $15.00 USD Received 22 Feb 2013; revised 17 May 2013; accepted 17 May 2013; published 24 May 2013

design. These differences can be compensated by choosing proper lengths of optical patch cords, or by using digital signal processing.

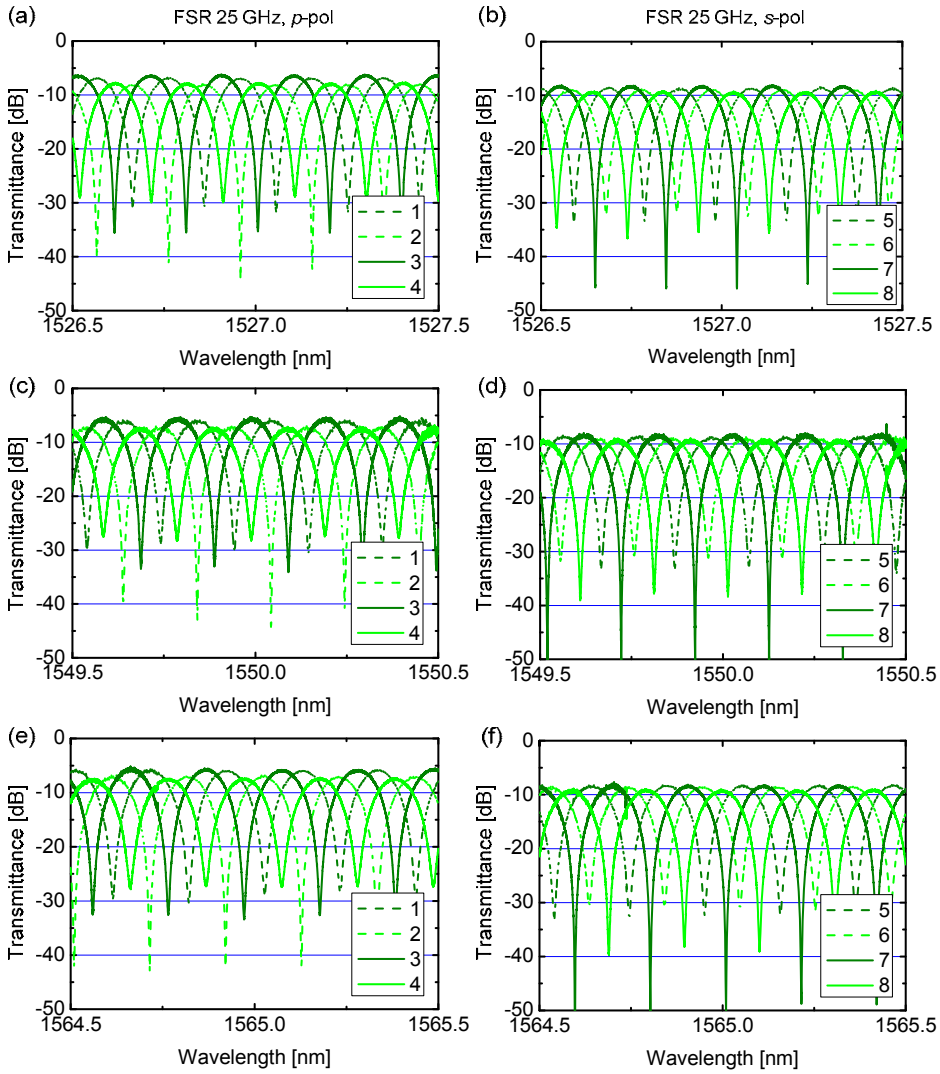

Fig. 5. Micro-optical interferometer as self-coherent receiver. Spectral responses at outputs 1 (dark green dashed line), 2 (light green dashed line), 3 (dark green solid line) and 4 (light green solid line) for *p*-polarization and FSR = 25 GHz. Wavelength range (a) 1526.5…1527.5 nm, (c) 1549.5 …1550.5 nm, (e) 1564.5…1565.5 nm. Spectral responses of outputs 5 (dark green dashed line), 6 (light green dashed line), 7 (dark green solid line) and 8 (light green solid line) at *s*-polarization and FSR = 25 GHz. Wavelength ranges (b) 1526.5…1527.5 nm and (d) 1549.5…1550.5 nm, (f) 1564.5…1565.5 nm.

Finally, we tested the micro-optical interferometer with real data by receiving a 28 GBd PolMUX QPSK signal. The experimental setup is depicted in Fig. 6(a). A PolMUX QPSK signal is connected directly to the micro-optical interferometer via an erbium-doped fiber amplifier (EDFA) stage and an optical filter. The input polarization states at the input of the receiver are aligned with the polarization states at the transmitter so that no digital signal processing is required to demultiplex the polarizations. The signals are then received with four pairs of balanced detectors, and then sent to two real-time sampling scopes (Agilent optical modulation analyzer having a sampling rate of 80 GSa/s and a bandwidth of 32 GHz).

#185858 - $15.00 USD Received 22 Feb 2013; revised 17 May 2013; accepted 17 May 2013; published 24 May 2013

No digital equalizer was applied. First, the micro-optical interferometer is configured as a self-coherent receiver. The constellation diagrams of the received signal in both polarizations are presented in Fig. 6(b). The signal quality is quantified with error vector magnitude (EVM) measurements. A value of EVM = 15% is found, which is comparable with the signal quality for commercial devices. Second, the micro-optical interferometer is configured as a coherent receiver. The associated constellation diagrams are presented in Fig. 6(c), and the measured EVM are about 16%. The slightly worse performance of the coherent receiver is mostly due to the finite polarization extinction ratio and the insertion loss difference as shown in Table 2. This can be improved by using better-quality waveplates.

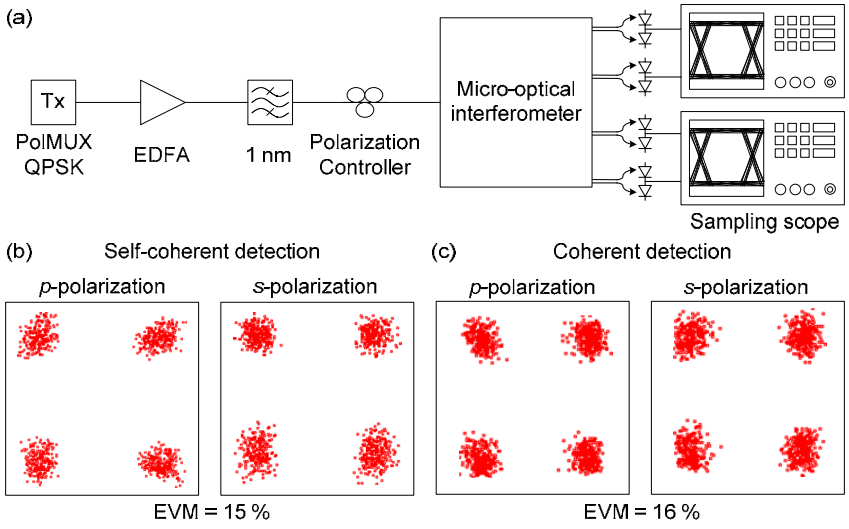

Fig. 6. Experimental setup and results for self-coherent and coherent receivers with the micro-optical interferometer serving as a frontend. (a) Schematic of the experiment setup. (b) Constellation diagrams of the signals received by a self-coherent receiver. (c) Constellation diagrams of the signals received by a coherent receiver.

5. Conclusion

We presented a micro-optical interferometer that can be switched between a self-coherent receiver and a coherent receiver. It folds four delay interferometers and two optical 90° hybrids into one single interferometer structure. With the help of a LIGA fabricated micro-optical bench, the four-in-one interferometer can be implemented on a 21 × 22 mm^2 chip with commercial available components. We measured excellent optical performance. Its function as a self-coherent and a coherent receiver frontend has been validated experimentally with a 112 Gbit/s PolMUX QPSK signal.

Appendix: Theory of the interferometer frontend

Coherent Receiver. The operation principle of the coherent receiver is explained by using the Jones calculus. As an example, consider the configuration in Fig. 1(e). At the input we have electric fields of the signal (blue line) and LO (red line),

$$\vec{E}_{sig} = \begin{bmatrix} E_{sig\text{-}s} \\ E_{sig\text{-}p} \end{bmatrix} = \begin{bmatrix} A_{sig\text{-}s} e^{j\omega_{sig}t} \\ A_{sig\text{-}p} e^{j\omega_{sig}t} \end{bmatrix}, \quad \vec{E}_{LO} = \begin{bmatrix} E_{LO\text{-}s} \\ E_{LO\text{-}p} \end{bmatrix} = \begin{bmatrix} A_{LO\text{-}s} e^{j\omega_{LO}t} \\ A_{LO\text{-}p} e^{j\omega_{LO}t} \end{bmatrix}. \tag{1}$$

The signal and LO are split by two separate PBSs in two orthogonal polarizations (transmitted beam in *p*-polarization, dashed line, and reflected beam in *s*-polarization, solid line). The two spatially separated beams enter the non-polarizing beam-splitter (NPBS) where they are

#185858 - $15.00 USD Received 22 Feb 2013; revised 17 May 2013; accepted 17 May 2013; published 24 May 2013

equally split in two paths. We now focus on the respective optical paths with a particular polarization, namely *p*-polarization (dashed blue line) for the signal, and *s*-polarization (red solid line) for the LO, point A in Fig. 1(e). We assume that all the components are ideal, and that there is a phase shift of '–j' between the reflected and transmitted beams after the PBS1 as well as after the NPBS. Omitting the propagator, the beam on the upper path after passing the NPBS (point B) can be written as

$$\begin{bmatrix} E_s^B \\ E_p^B \end{bmatrix} = \frac{1}{\sqrt{2}} \begin{bmatrix} 1 & 0 \\ 0 & 1 \end{bmatrix}_{\text{NPBS}} \cdot \begin{bmatrix} -\text{j}E_{LO\text{-}s} \\ E_{sig\text{-}p} \end{bmatrix} = \frac{1}{\sqrt{2}} \begin{bmatrix} -\text{j}E_{LO\text{-}s} \\ E_{sig\text{-}p} \end{bmatrix}. \tag{2}$$

This beam passes through a half waveplate (HWP). The axes of the half waveplate are at an angle of –45° with respect to the axes of the PBSs. It flips the polarization of the signal and LO to their orthogonal states. The field after the HWP at point C in Fig. 1(e) is

$$\begin{bmatrix} E_s^C \\ E_p^C \end{bmatrix} = \begin{bmatrix} 0 & 1 \\ 1 & 0 \end{bmatrix}_{\text{HWP}-45^\circ} \cdot \frac{1}{\sqrt{2}} \begin{bmatrix} -\text{j}E_{LO\text{-}s} \\ E_{sig\text{-}p} \end{bmatrix} = \frac{1}{\sqrt{2}} \begin{bmatrix} E_{sig\text{-}p} \\ -\text{j}E_{LO\text{-}s} \end{bmatrix}. \tag{3}$$

The beam is then reflected and passes through a quarter waveplate (QWP). Because magnitude and phase introduced by the two reflectors in the two paths are same, their influences cancel when the two beams interfere, so we omit the reflectors in our calculation. The axes of the QWP are aligned to the axes of the signal and LO. The QWP adds a 90° phase shift for one polarization (here, the *s*-polarization) so that the signal can be superimposed with an in-phase LO and quadrature-phase LO separately. The field at point D in Fig. 1(e) is

$$\begin{bmatrix} E_s^D \\ E_p^D \end{bmatrix} = \begin{bmatrix} \text{j} & 0 \\ 0 & 1 \end{bmatrix}_{\text{QWP}0^\circ} \cdot \frac{1}{\sqrt{2}} \begin{bmatrix} E_{sig\text{-}p} \\ -\text{j}E_{LO\text{-}s} \end{bmatrix} = \frac{1}{\sqrt{2}} \begin{bmatrix} \text{j}E_{sig\text{-}p} \\ -\text{j}E_{LO\text{-}s} \end{bmatrix}. \tag{4}$$

The electric field on the right hand side of point E in Fig. 1(e) is

$$\begin{bmatrix} E_s^E \\ E_p^E \end{bmatrix} = \frac{-\text{j}}{\sqrt{2}} \begin{bmatrix} 1 & 0 \\ 0 & 1 \end{bmatrix}_{\text{NPBS}} \cdot \begin{bmatrix} -\text{j}E_{LO\text{-}s} \\ E_{sig\text{-}p} \end{bmatrix} = \frac{1}{\sqrt{2}} \begin{bmatrix} -E_{LO\text{-}s} \\ -\text{j}E_{sig\text{-}p} \end{bmatrix}. \tag{5}$$

The beams are then reflected back onto the NPBS, where the signal and LO beams are superimposed at point F. Both the I and the Q signals interfere constructively (destructively) with the correspondingly polarized LO field. At outputs in Fig. 1(e),

$$\begin{bmatrix} E_{\Delta\text{I}\text{-}p} \\ E_{\Delta\text{Q}\text{-}p} \end{bmatrix} = \frac{1}{2} \begin{bmatrix} -\text{j}\left(E_{sig\text{-}p} - E_{LO\text{-}s}\right) \\ -\text{j}\left(E_{sig\text{-}p} - \text{j}E_{LO\text{-}s}\right) \end{bmatrix}, \quad \begin{bmatrix} E_{\Sigma\text{I}\text{-}p} \\ E_{\Sigma\text{Q}\text{-}p} \end{bmatrix} = \frac{1}{2} \begin{bmatrix} E_{sig\text{-}p} + E_{LO\text{-}s} \\ -\left(E_{sig\text{-}p} + \text{j}E_{LO\text{-}s}\right) \end{bmatrix}. \tag{6}$$

The in-phase and quadrature phase of the output beams are orthogonally polarized and subsequently separated by PBSs. At the four outputs the typical relations for an optical 90° hybrid are to be seen, $E_{sig\text{-}p} + E_{LO\text{-}s}$ and $E_{sig\text{-}p} - E_{LO\text{-}s}$ for the in-phase component, and $E_{sig\text{-}p} + \text{j}E_{LO\text{-}s}$ and $E_{sig\text{-}p} - \text{j}E_{LO\text{-}s}$ for the quadrature-phase component.

The relation for the *s*-polarization of the signal and *p*-polarization of LO can be deduced in the same way. Assuming the mirror cube in the left corner will introduce a phase shift π between *s* and *p*-polarizations, the resulting field at the outputs in Fig. 1(e) are

$$\begin{bmatrix} E_{\Sigma\text{I}\text{-}s} \\ E_{\Delta\text{Q}\text{-}s} \end{bmatrix} = \frac{1}{2} \begin{bmatrix} -\text{j}\left(E_{sig\text{-}s} + E_{LO\text{-}p}\right) \\ E_{sig\text{-}s} - \text{j}E_{LO\text{-}p} \end{bmatrix}, \quad \begin{bmatrix} E_{\Delta\text{I}\text{-}s} \\ E_{\Sigma\text{Q}\text{-}s} \end{bmatrix} = \frac{1}{2} \begin{bmatrix} -\left(E_{sig\text{-}s} - E_{LO\text{-}p}\right) \\ \text{j}\left(E_{sig\text{-}s} + \text{j}E_{LO\text{-}p}\right) \end{bmatrix}. \tag{7}$$

#185858 - $15.00 USD Received 22 Feb 2013; revised 17 May 2013; accepted 17 May 2013; published 24 May 2013

Thus in this polarization and phase diverse coherent receiver two optical 90° hybrids are nested in one physical device.

Self-coherent receiver. For a self-coherent receiver, the input has again two orthogonal polarizations,

$$\vec{E}_{sig} = \begin{bmatrix} E_{sig\text{-}s} \\ E_{sig\text{-}p} \end{bmatrix}. \tag{8}$$

The signal is split at PBS1, and both polarizations are further split at NPBS in two paths. The upper path has a time delay τ with respect to the path on the right hand side. After the NPBS, both beams pass a quarter waveplate (QWP). The axes of the QWPs (in white) are at a –45° angle with respect to the optical axes of the PBSs, so that they convert the linear polarizations (*s* and *p*) into circular polarizations. Taking for example the *s*-polarization (solid line), we find at point A, (the symbol '*' denotes the convolution operator)

$$\begin{aligned} \begin{bmatrix} E_s^A \\ E_p^A \end{bmatrix} &= \delta(t-\tau) * \left\{ \frac{1}{2}\begin{bmatrix} 1+\mathrm{j} & 1-\mathrm{j} \\ 1-\mathrm{j} & 1+\mathrm{j} \end{bmatrix}_{\mathrm{QWP}-45^\circ} \cdot \frac{1}{\sqrt{2}}\begin{bmatrix} 1 & 0 \\ 0 & 1 \end{bmatrix}_{\mathrm{NPBS}} \cdot \begin{bmatrix} \mathrm{j}E_{sig\text{-}s}(t) \\ 0 \end{bmatrix} \right\} \\ &= \frac{E_{sig\text{-}s}(t-\tau)}{2\sqrt{2}}\begin{bmatrix} -1+\mathrm{j} \\ 1+\mathrm{j} \end{bmatrix}. \end{aligned} \tag{9}$$

In order to superimpose the signal with its I and Q delayed copy, in Fig. 1(j) another quarter waveplate (gray) at an angle of 0° to the optical axes of PBSs intercepts the upper path. It introduces a relative 90° phase shift between the two polarizations in the same beam. Omitting the common propagator for the two paths, we have at point B in Fig. 1(j)

$$\begin{bmatrix} E_s^B \\ E_p^B \end{bmatrix} = \begin{bmatrix} \mathrm{j} & 0 \\ 0 & 1 \end{bmatrix}_{\mathrm{QWP0}^\circ} \cdot \frac{E_{sig\text{-}s}(t-\tau)}{2\sqrt{2}}\begin{bmatrix} -1+\mathrm{j} \\ 1+\mathrm{j} \end{bmatrix} = \frac{E_{sig\text{-}s}(t-\tau)}{2\sqrt{2}}\begin{bmatrix} -1-\mathrm{j} \\ 1+\mathrm{j} \end{bmatrix}. \tag{10}$$

The beam on the right path goes through a QWP under –45°as well. At point C we find

$$\begin{bmatrix} E_s^C \\ E_p^C \end{bmatrix} = \frac{1}{2}\begin{bmatrix} 1+\mathrm{j} & 1-\mathrm{j} \\ 1-\mathrm{j} & 1+\mathrm{j} \end{bmatrix}_{\mathrm{QWP}-45^\circ} \cdot \frac{-\mathrm{j}}{\sqrt{2}}\begin{bmatrix} 1 & 0 \\ 0 & 1 \end{bmatrix}_{\mathrm{NPBS}} \cdot \begin{bmatrix} \mathrm{j}E_{sig\text{-}s}(t) \\ 0 \end{bmatrix} = \frac{E_{sig\text{-}s}(t)}{2\sqrt{2}}\begin{bmatrix} 1+\mathrm{j} \\ 1-\mathrm{j} \end{bmatrix}. \tag{11}$$

Therefore in each beam the powers of the new *s* and *p*-polarizations (referred to the PBSs axes) are equal. Birefringent elements other than QWP can also be used as long as the powers of the new *s* and *p*-polarized fields are equal.

The delayed and undelayed beams are then superimposed in the NPBS. The fields at the outputs are

$$\begin{aligned} \begin{bmatrix} E_{\Delta\mathrm{Q}\text{-}s}(t) \\ E_{\Delta\mathrm{I}\text{-}s}(t) \end{bmatrix} &= \frac{e^{-\mathrm{j}135^\circ}}{2\sqrt{2}}\begin{bmatrix} E_{sig\text{-}s}(t) - \mathrm{j}E_{sig\text{-}s}(t-\tau) \\ E_{sig\text{-}s}(t) - E_{sig\text{-}s}(t-\tau) \end{bmatrix}, \\ \begin{bmatrix} E_{\Sigma\mathrm{Q}\text{-}s}(t) \\ E_{\Sigma\mathrm{I}\text{-}s}(t) \end{bmatrix} &= \frac{e^{-\mathrm{j}45^\circ}}{2\sqrt{2}}\begin{bmatrix} E_{sig\text{-}s}(t) + \mathrm{j}E_{sig\text{-}s}(t-\tau) \\ E_{sig\text{-}s}(t) + E_{sig\text{-}s}(t-\tau) \end{bmatrix}. \end{aligned} \tag{12}$$

Therefore the output PBSs separate the two polarizations to retrieve the I and Q components of the input signal at *s*-polarization.

For the *p*-polarization of the input signal (dashed blue line), we measure its I and Q components at the outputs as indicated

#185858 - $15.00 USD Received 22 Feb 2013; revised 17 May 2013; accepted 17 May 2013; published 24 May 2013

$$\begin{bmatrix} E_{\Delta Q\text{-}p}(t) \\ E_{\Delta I\text{-}p}(t) \end{bmatrix} = \frac{e^{j45^\circ}}{2\sqrt{2}} \begin{bmatrix} E_{sig\text{-}p}(t) - jE_{sig\text{-}p}(t-\tau) \\ -\left(E_{sig\text{-}p}(t) - E_{sig\text{-}p}(t-\tau)\right) \end{bmatrix},$$
$$\begin{bmatrix} E_{\Sigma Q\text{-}p}(t) \\ E_{\Sigma I\text{-}p}(t) \end{bmatrix} = \frac{e^{j135^\circ}}{2\sqrt{2}} \begin{bmatrix} E_{sig\text{-}p}(t) + jE_{sig\text{-}p}(t-\tau) \\ -\left(E_{sig\text{-}p}(t) + E_{sig\text{-}p}(t-\tau)\right) \end{bmatrix}. \quad (13)$$

Thus, in self-coherent receiver, four delay interferometers (I and Q for each of the two polarizations *s* and *p*) are spatially folded into one single delay interferometer and share the same time delay and phase shifter.

With the tunable delay and the adjustable liquid crystals, the receiver frontend can be easily switched between coherent and self-coherent receptions without replacing any component. Naturally, for coherent reception a LO has to be added.

Acknowledgment

This work is supported by the European Commission's Network of Excellence EuroFOS and by the Karlsruhe School of Optics and Photonics (KSOP). We further acknowledge support by Deutsche Forschungsgemeinschaft (DFG) and Open Access Publishing Fund of Karlsruhe Institute of Technology (KIT). X-ray lithography has been carried out at the Karlsruhe Nano Micro Facility (KNMF, www.kit.edu/knmf), a Helmholtz Research Infrastructure at Karlsruhe Institute of Technology (KIT, www.kit.edu).